ECTI Transactions on Computer and Information Technology
Journal homepage: https://ph01.tci-thaijo.org/index.php/ecticit/
Published by the ECTI Association, Thailand, ISSN: 2286-9131

A Mathematical Model and PI Controller Design Based on Indirect Vector Control for Permanent Magnet Synchronous Motor

Nutthawut Kongchoo[1], Phonsit Santiprapan[2] and Nattha Jindapetch[3]

ABSTRACT

A mathematical model of a permanent magnet synchronous motor (PMSM) is necessary to design the control of PMSM drives. The mathematical model of a three-phase system is not commonly used for control design since this approach is a time-varying model. As a result, control strategy design becomes even more difficult. Due to this problem, this paper presents a dynamic model of the PMSM using the dq modeling method. The dynamic model derived in this work has been validated with the exact topology model in the MATLAB/Simulink program. In addition, this model is applied to designing the indirect vector control for a PMSM drive. The speed and the current control loops based on the PI controller are considered. The simplified design approach for the PMSM drives is presented in this paper. The simulation results show that the proposed controller design can accurately regulate the actual speed obeying the command speed. The speed accuracy is up to 99.97% in the load torque changes and 99.98% in the command speed changes.

Article information:

Keywords: Permanent Magnet Synchronous Motor (PMSM), *dq* Modelling Method, Model Validation, Indirect Vector Control, PI Controller Design

Article history:
Received: May 16, 2021
Revised: July 17, 2021
Accepted: September 6, 2021
Published: June 18, 2022 (Online)

DOI: 10.37936/ecti-cit.2022163.245351

1. INTRODUCTION

Nowadays, permanent magnet synchronous motors (PMSM) are widely used for many industrial applications such as electric equipment, conveyor belts, robot arms, and especially for electric vehicles (EV). A PMSM has more efficiency, higher torque to inertia ratio, lower noise, and more robustness than an induction motor (IM) [1]. To operate a PMSM, the speed and torque of the PMSM must be suitably controlled under desired conditions. The development of a PMSM drive system is therefore a critical issue [3]. In a traditional drive system, scalar control methods (such as V/F control, flux control, etc.) have been applied to motor drives [2]. This method is simple. It can be implemented using analogue circuits. Based on a review of relevant literature [3–10], the scalar control method is not recommended because the tracking error of the control system from this method is considered an AC signal (both the magnitude and frequency). Consequently, the controller has become more difficult to implement for regulating the PMSM speed and torque.

A vector control method [3–4] has been applied to motor drives in order to achieve high performance PMSM drives. This approach can be divided into two categories: direct vector [4] and indirect vector controls [3]. Direct vector control requires rotor flux measurement to calculate the control signal. It has important limitations, including installation costs and complexity. The indirect vector control is the focus of this work. This is typically called field-oriented control (FOC). This control does not require rotor flux measurement. The installation of a sensor and control design is less complicated compared with direct vector control. The control signal is generated by the motor parameter calculation. In this control operation, the synchronous frame (dq-axis) is used as a reference axis. The d and q-axis currents are the instantaneous stator current vectors. It can be decomposed into flux and torque-producing currents. There are two control loops: flux and torque control loops. For this control strategy, the tracking error of the control loop is considered a DC signal. This signal is easy to compensate for using a controller, especially a proportional-integral (PI) controller. Theoretically,

[1,2,3] The authors are with Department of Electrical Engineering, Faculty of Engineering, Prince of Songkla University (PSU), Songkhla, Thailand, E-mail: gotgot1@hotmail.com, phonsit.s@psu.ac.th and nattha.s@psu.ac.th
[2] The corresponding author: phonsit.s@psu.ac.th

a PI controller can reduce the steady state error of the DC components (the fundamental value) to zero. As mentioned, the mathematical model of PMSM on the dq-axis is necessary for the control design. Due to the benefit of fundamental study, this paper presents how to derive the mathematical model of PMSM using the dq modeling approach.

The objective of this work is to control the PMSM speed to be equal to the command speed. Previous related works have focused on several controllers such as proportional-integral-derivative control (PID) [5], fuzzy logic control (FLC) [3], iterative learning control (ILC) [6], sliding mode control (SMC) [7], predictive current control (PCC) [8], and model predictive current control (MPCC) [9]. However, the operation of those controllers is more difficult and complicated. A large computational capability is required for those digital controls. For this work, a simple controller is an interesting approach to develop. As mentioned earlier, the PI controller [10] is suitable for indirect vector control. This controller can provide a small steady state error. It is enough to accurately control the PMSM speed. In order to avoid a large computational burden, control design complexity, and difficulty in real implementation, a simplified controller design is proposed in this paper.

This paper is structured as follows. The principle and mathematical model of the PMSM are briefly explained in Section 2. The PMSM model validation is expressed in Section 3. Section 4 presents the PI parameters design of indirect vector control. The simulation results of the PMSM speed control are shown in Section 5. Finally, Section 6 concludes this paper.

2. PRINCIPLE AND MATHEMATICAL MODEL OF PMSM

The operation of a PMSM is similar to that of a three-phase induction motor. The three-phase voltage source connected to the stator winding produces a rotating magnetic field (RMF). The RMF causes the rotor to turn. Power losses on the rotor side do not occur because the rotor of a PMSM is a permanent magnet. Moreover, this machine can provide constant torque. The structure and equivalent circuit of the PMSM are shown in Fig. 1. The system parameters are described in Table 1.

The *dq* modeling method is applied to derive a mathematical model of the system as depicted in Fig. 1. The *dq*–axis in Fig. 2 is rotated with the angular speed (ω_r). The stator voltages ($v_{s(abc)}$) can be written for a three-phase system as (1).

$$v_{s(abc)} = R_S i_{S(abc)} + \frac{d}{dt}\left(L_s i_{S(abc)} + \lambda_{pm}(\theta)\right) \quad (1)$$

Where the $\frac{d}{dt}\lambda_{pm}(\theta)$ in (1) is the back EMF as shown in (2). Then, the mathematical model of the three-phase system in (3) can be transformed into the *dq*-axis. The dynamic equation of the PMSM on *dq*-axis can be written as shown in (4)-(5).

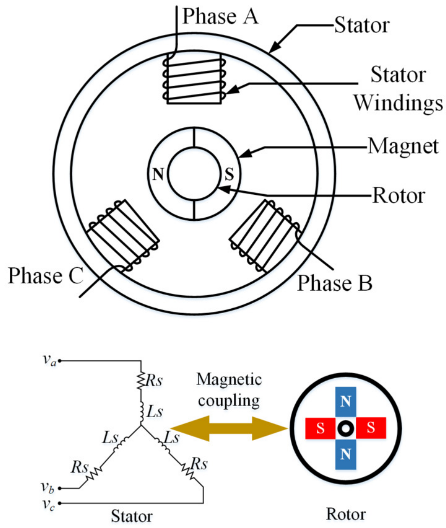

Fig.1: *Structure and equivalent circuit of PMSM.*

$$\frac{d}{dt}\lambda_{pm}(\theta) = -\omega_r\lambda_{pm}\begin{bmatrix} \sin(\theta_r) \\ \sin(\theta_r - 2\pi/3) \\ \sin(\theta_r + 2\pi/3) \end{bmatrix} \quad (2)$$

Table 1: *List of symbols.*

Symbol	Meaning
$v_{S(abc)}, v_{Sa}, v_{Sb}$ v_{Sc}	three-phase stator voltage
$v_{Sd}, v_{Sq}, v_{s(dq)}$	stator voltage on dq-axis
v^*_{Sd}, v^*_{Sq}	reference stator voltage on dq-axis
$i_{S(abc)}, i_{Sa}, i_{Sb}, i_{Sc}$	three-phase stator current
i_{Sd}, I_{Sd}	stator current on d-axis
i^*_{Sd}, I^*_{Sd}	reference stator current on d-axis
i_{Sq}, I_{Sq}	stator current on q-axis
i^*_{Sq}, I^*_{Sq}	reference stator current on q-axis
L_s	stator inductance
L_d, L_q, L_{dq}	inductance on *dq*-axis
R_s	stator resistance
λ_{pm}	permanent magnet flux
λ_d, λ_q	permanent magnet flux on *dq*-axis
θ_r, ω_r	electrical angular position and electrical angular speed
θ_m, ω_m	angular position and angular speed
τ_e, τ_L	developed torque, load torque
B	viscous friction coefficient
J	rotor inertia
P	number of poles
τ_{dq}	time constant (L_{dq}/R_S)
k_τ	torque constant ($\left(\frac{3}{2}\right)\left(\frac{P}{2}\right)\lambda_{pm}$)
$\omega_{ni}, \omega_{n\omega}$	natural frequency for the current loop and natural frequency for the speed loop
ζ_i, ζ_ω	damping ratio for the current loop and damping ratio for the speed loop
$K_{PC,(dq)}, K_{P\omega}$	proportional gain
$K_{IC,(dq)}, K_{I\omega}$	integral gain

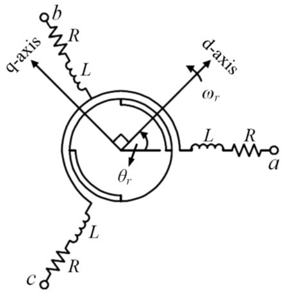

Fig.2: *Vector diagram of the dq-axis.*

$$\left.\begin{aligned} v_{Sa} &= R_S i_{Sa} + L_s \frac{d}{dt} i_{Sa} - \omega_r \lambda_{pm} \sin(\theta_r) \\ v_{Sb} &= R_S i_{Sb} + L_s \frac{d}{dt} i_{Sb} - \omega_r \lambda_{pm} \sin(\theta_r - 2\pi/3) \\ v_{Sc} &= R_S i_{Sc} + L_s \frac{d}{dt} i_{Sc} - \omega_r \lambda_{pm} \sin(\theta_r + 2\pi/3) \end{aligned}\right\} \quad (3)$$

$$\left.\begin{aligned} v_{Sd} &= R_S i_{Sd} - \omega_r \lambda_q \frac{d}{dt} \lambda_d \\ v_{Sq} &= R_S i_{Sq} + \omega_r \lambda_d \frac{d}{dt} \lambda_q \end{aligned}\right\} \quad (4)$$

Substituting the $\lambda_d = L_d i_{Sd} + \lambda_{pm}$ and $\lambda_q = L_q i_{Sq}$ into (4) yields (5).

$$\left.\begin{aligned} v_{Sd} &= R_S i_{Sd} + L_d \frac{d}{dt} i_{Sd} - \omega_r L_q i_{Sq} + \frac{d}{dt} \lambda_{pm} \\ v_{Sq} &= R_S i_{Sq} + L_d \frac{d}{dt} i_{Sq} - \omega_r L_d i_{Sd} + \omega_r \lambda_{pm} \end{aligned}\right\} \quad (5)$$

As a result, the equivalent circuit of PMSM in dq-axis derived by using the dq modeling method is shown in Fig. 3.

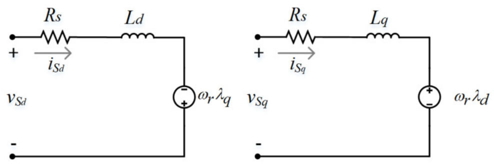

Fig.3: *Equivalent circuit in the dq-axis.*

From the PMSM model, the developed torque equation of the PMSM is given in (6).

$$\tau_e = \left(\tfrac{3}{2}\right)\left(\tfrac{P}{2}\right)(\lambda_d i_{Sq} - \lambda_q i_{Sd}) = \left(\tfrac{3P}{4}\right)(\lambda_{pm} i_{Sq} + (L_d - L_q) i_{Sd} i_{Sq}) \quad (6)$$

Due to the relationship between torque (τ_e), the angular speed (ω_m), and the angular position (θ_m) of the PMSM as shown in Fig. 4, the τ_e, ω_m and θ_m can be calculated as shown in (7)-(9).

$$\tau_e = \tau_L + B\omega_m + J \frac{d}{dt} \omega_m \quad (7)$$

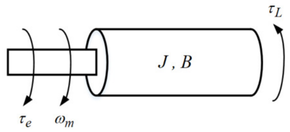

Fig.4: *Mechanical motion of PMSM.*

$$\omega_m = \int ((\tau_e - \tau_L - B\omega_m)/J) dt \quad (8)$$

$$\omega_r = \left(\frac{P}{2}\right) \omega_m = \frac{d}{dt} \theta_r \Rightarrow \theta_m = \left(\frac{2}{P}\right) \theta_r \quad (9)$$

3. PMSM MODEL VALIDATION

In the previous section, in order to design the control scheme and the PI controller parameters, the differential equations of the PMSM torque and speed are verified. The simulation for model validation uses the exact topology model in SimPowerSystem of MATLAB/Simulink called the benchmark model. The PMSM parameters in Fig. 1 are given in Table 2. These parameters are cited from the real PMSM (4 pole pairs, 750 W, 3000 rpm). These PMSM parameters in Table 2 have been tested [11]. The proposed model implemented by MATLAB/Simulink is illustrated in Fig. 5.

Table 2: *Parameters of PMSM.*

Symbol	Description	Value
R_S	Stator resistance	0.55Ω
L_d, L_q	Inductance on dq-axis	16.61 mH, 16.22 mH
λ_{pm}	Permanent magnet flux	0.121 Vs
J	Rotor inertia	$7.246\text{x}\times10^{-}3$ kg.m^2
P_{pair}	Pole pair	4
P_S, N_S	Rated power, speed	750 W, 3000 rpm

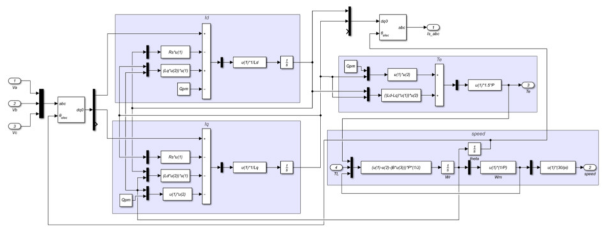

Fig.5: *Simulation model used to validate the mathematical model of the PMSM.*

The testing conditions for model validation consist of the load torque and the voltage per frequency changing. Fig. 6 shows the response comparison of the PMSM torque and speed between the dq model and the benchmark model, which are detailed as presented in Tables 3 and 4, respectively. The simulation results confirm that the dynamic model derived

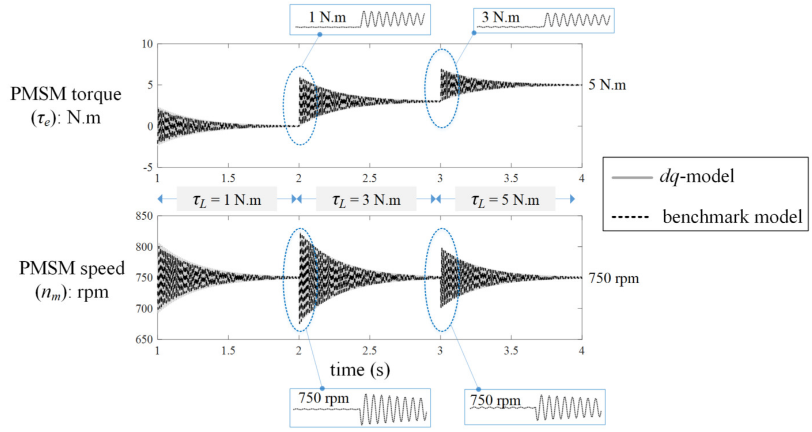

(a) Load torque change

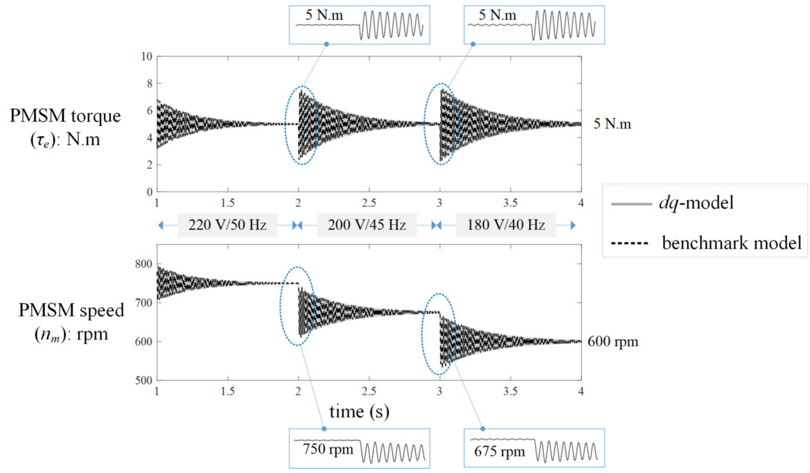

(b) Voltage per frequency control change

Fig.6: *PMSM torque and PMSM speed responses.*

Table 3: *Model validation for changing the load torque.*

Approach	Stator voltage ($v_{s(abc)}$: V_{rms})	Frequency (f_s : Hz)	Load torque (τ_L : N.m)	Measured values	
				Speed (n_m : rpm)	Torque (τ_e : N.m)
dq-model	220	50	1	750	1
benchmark				750	1.04
dq-model			3	750	3
benchmark				750	3.04
dq-model			5	750	5
benchmark				750	5.04

Table 4: *Model validation for changing the voltage per frequency control.*

Approach	Stator voltage ($v_{s(abc)}$: V_{rms})	Frequency (f_s : Hz)	Load torque (τ_L : N.m)	Measured values	
				Speed (n_m : rpm)	Torque (τ_e : N.m)
dq-model	220	50	5	750	5
benchmark				750	5.04
dq-model	200	45		675	5
benchmark				675	5.04
dq-model	180	40		600	5
benchmark				600	5.03

by the dq modeling method represents the same behaviour as the benchmark model. From validation results, this model can be applied for indirect vector control design.

4. DESIGN OF INDIRECT VECTOR CONTROL

From (5) to (6), the stator voltage ($v_{s(dq)}$) and torque (τ_e) on the dq-axis are considered for the indirect vector control design. The dq-axis is rotated at the synchronous speed of the PMSM. The d-axis is aligned along with the flux control. Here, the PMSM speed and torque can be controlled on the q-axis. The indirect vector control scheme of the PMSM drive is shown in Fig. 7. For this control strategy, the flux vector must be kept synchronized with the rotor magnetic poles [7]. Therefore, the reference current on the d-axis (i_d^*) is set to zero. The indirect vector control consists of the current and speed control loops.

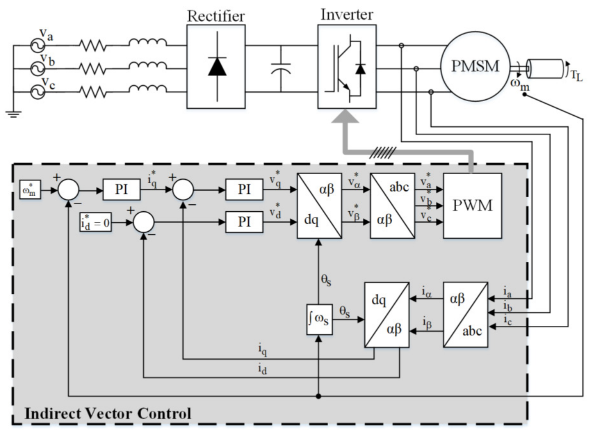

Fig.7: *Indirect vector control scheme of PMSM drive.*

4.1 Design of the Current Control Loop

The differential equation from (5) is transformed to the frequency domain by taking the Laplace transformation. The block diagram of the current control based on PI controllers is depicted in Fig. 8.

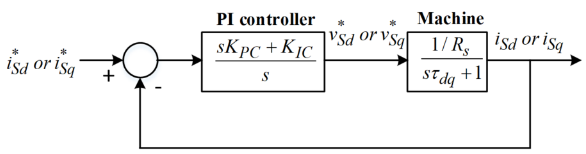

Fig.8: *Block diagram of the current control loop.*

From Fig. 8, the closed-loop transfer function of the current control can be derived from (10). The parameters of PI controllers ($K_{PC,d}, K_{IC,d}, K_{PC,q}, K_{IC,q}$) can be calculated by comparing them with the denominator of the standard second order characteristic equation as shown in (11).

$$\frac{I_{Sd}(s)}{I_{Sd}^*(s)}=\frac{I_{Sq}(s)}{I_{Sq}^*(s)}=\frac{(sK_{PC,(dq)}+K_{IC,(dq)}/R_S\tau_{dq})}{s^2+\left(\frac{R_S+K_{PC,(dq)}}{R_S\tau_{dq}}\right)s+\left(\frac{K_{IC,(dq)}}{R_S\tau_{dq}}\right)} \tag{10}$$

$$T_C(s)=\frac{\omega_{ni}^2}{s^2+2\zeta_i\omega_{ni}s+\omega_{ni}^2} \tag{11}$$

where:

ω_{ni} is equal to 100π rad/s

ζ_i is equal to 0.8

4.2 Design of the Speed Control Loop

From (6) to (7), the block diagram of the speed control based on the PI controller is illustrated in Fig. 9. The closed loop transfer function for speed control can be derived from (12). The denominator comparison between (12) and (13) is used to calculate the PI controller parameters ($K_{P\omega}, K_{I\omega}$).

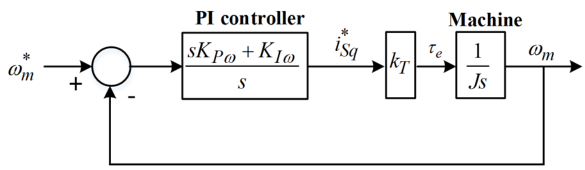

Fig.9: *Block diagram of the speed control loop.*

$$\frac{\omega_m(s)}{\omega_m^*(s)}=\frac{k_\tau(sK_{P\omega}+K_{I\omega})/J}{s^2+\left(\frac{k_\tau K_{P\omega}}{J}\right)s+\left(\frac{k_\tau K_{I\omega}}{J}\right)} \tag{12}$$

$$T_\omega(s)=\frac{\omega_{n\omega}^2}{s^2+2\zeta_\omega\omega_{n\omega}s+\omega_{n\omega}^2} \tag{13}$$

where:

$\omega_{n\omega}$ is equal to 20π rad/s

ζ_ω is equal to 0.8

The PI controller parameters for the indirect vector control are given in Table 5. The root locus of the closed loop control system in the s-domain is shown in Fig. 10. The desired dominant poles of the closed loop systems are located in the stable region (the left-hand side of the s-plane). This means that the control system remains the operating point stable.

Table 5: *PI controller parameters of the indirect vector control for PMSM drive.*

Control loop	Proportional gain	Integral gain
Current control	$K_{PC,(dq)}$= 7.80	$K_{IC,(dq)}$= 1639.34
Speed control	$K_{P\omega}$ = 0.10	$K_{I\omega}$= 3.94

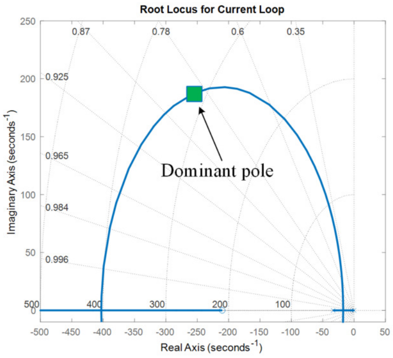

(a) Current control loop

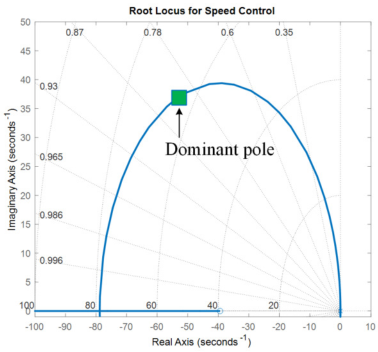

(b) Speed control loop

Fig.10: *Root locus of the closed loop control system.*

5. SIMULATION RESULTS AND DISCUSSION

The speed control performance of PMSM under indirect vector control was verified by the MATLAB/ Simulink model in Fig. 11. For the PMSM utilization, the torque capability and the speed control accuracy are therefore considered. The performance of the PI controller parameters designed in Section 4 was tested in two cases, when load torque and speed are changing. The simulation results are shown in Figs. 12 to 13.

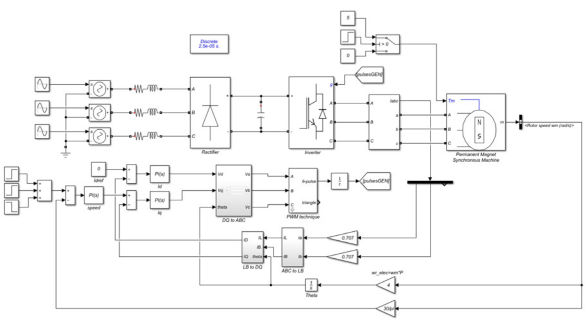

Fig.11: *Simulation model used to verify the performance.*

5.1 Speed control performance of changing the load torque

According to Fig. 12, the PMSM speed is controlled to maintain a constant speed of 1000 rpm.

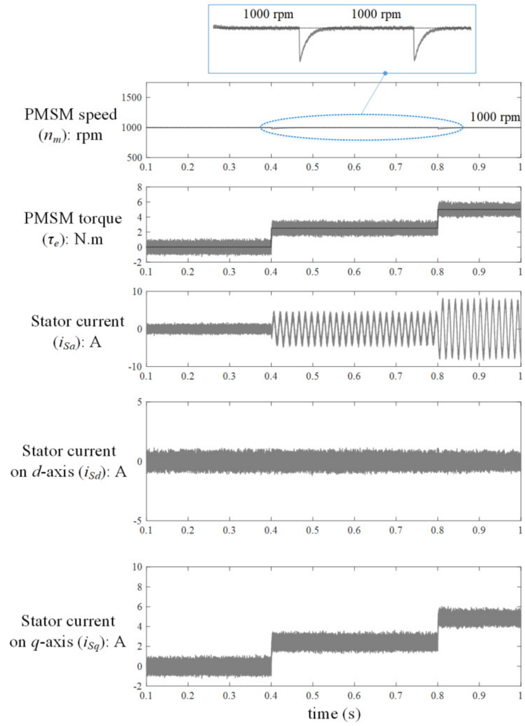

Fig.12: *Response to a step change of load torque.*

Then, the load torque (τ_L) is increased from no-load to 2.5 N·m at t = 0.4 s. It is obvious that when the load torque is increased, the PMSM speed (n_m) initially decreases. However, the speed control can regulate the n_m at the desired speed ($n_m^* = 1000$ rpm). The PMSM torque (τ_e) and the stator currents ($i_{S(abc)}$) will increase according to the increase of load torque. At t = 0.8, the load torque is increased from 2.5 to 5 N·m. It can be seen that the PMSM drive system can maintain the n_m at the n_m^* . The root mean square error between the desired values (n_m^*, τ_L^*) and actual values (n_m, τ_L) is used as the tracking errors (E_{speed}, E_{torque}) in (14) and (15), respectively. The N value is the data number. Tracking accuracy (A_{speed}, A_{torque}) can be defined by (16). The tracking performance is presented in Table 6. As a result, the speed control based on the PI controller can provide good accuracy.

$$E_{speed} = \sqrt{\frac{\sum |n_m^* - n_m|^2}{N}} \tag{14}$$

$$E_{torque} = \sqrt{\frac{\sum |\tau_L^* - \tau_L|^2}{N}} \tag{15}$$

$$
\begin{aligned}
A_{speed} &= 100\% - \left(\frac{E_{speed} \times 100\%}{n_m^*}\right) \\
A_{torque} &= 100\% - \left(\frac{E_{torque} \times 100\%}{\tau_L^*}\right)
\end{aligned} \tag{16}
$$

Table 6: *The tracking error and tracking accuracy performance indices under load torque change.*

Changing the load torque (N·m)	Tracking error		Tracking accuracy	
	E_{speed} (rpm)	E_{torque} (N·m)	A_{speed} (%)	A_{torque} (%)
No-load	0.3101	0.1979	99.97	80.21
2.5	0.2802	0.1823	99.97	92.71
5	0.3118	0.1679	99.97	96.64

For the responses of the stator current on dq-axis, the flux vector is controlled on d-axis. The i_{Sd} is nearly zero. It confirms that the PMSM can generate the developed torque. The i_{Sq} represents the speed and torque controls of PMSM. The i_{Sd} will increase the amplitude when the τ_L is increased.

5.2 Speed control performance of changing the command speed

For this case, the τ_L is kept constant at 5 N·m. From Fig. 13, the τ_e is controlled to be constant with the τ_L. The n_m^* is varied in three steps. First, the PMSM speed is controlled at 1000 rpm. Then the n_m^* is set to 1500 rpm at t = 0.4 s. At t=0.8 s, the n_m^* is adjusted to decrease the PMSM speed to 1000 rpm. The responses are shown in Fig. 13. The tracking error and tracking accuracy under speed change are shown in Table 7. These results confirm that the speed control based on the PI controller can still control the n_m following the n_m^* even though the n_m^* is suddenly varied.

Table 7: *The tracking error and tracking accuracy performance indices under speed change.*

Changing the commmand speed(rpm)	Tracking error		Tracking accuracy	
	E_{speed} (rpm)	E_{torque} (N·m)	A_{speed} (%)	A_{torque} (%)
1000	0.2713	0.1694	99.97	96.61
1500	0.2622	0.1269	99.98	97.46

The amplitude of $i_{S(abc)}$ is constant since τ_L is constant. The frequency of the $i_{S(abc)}$ is adjusted to correspond to the PMSM speed change. According to the waveform of the i_{Sa}, the frequency of the i_{Sa} will increase when the PMSM speed is increased. The current control loop on the dq-axis is sufficient to control the flux vector, torque, and speed. The i_{Sq} response is constant due to the constant τ_L. In order to test the transient performance of the PMSM drive system, the response to a step change of n_m^* is investigated. It can be seen that the τ_e and $i_{S(abc)}$ are

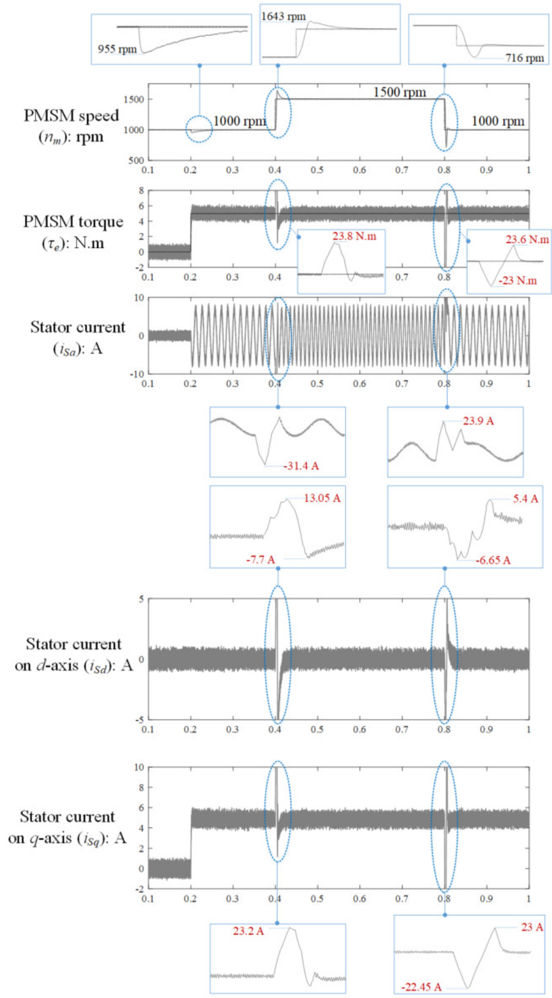

Fig.13: *Response to a step change of command speeds.*

highly oscillating waveforms in the short-term. This term produces the speed fluctuation and the motor vibration. These problems can cause equipment failure and will increase the power loss of the PMSM. The development of the PMSM drive system will continue to be studied in future work.

6. CONCLUSION

This paper presents how to derive a mathematical model of PMSM. The PMSM model is validated with the benchmark model from MATLAB/Simulink. The model verification confirms that the responses of PMSM speed and torque represent the same behaviour as the benchmark model. Therefore, the validated PMSM model can be used to design an indirect vector control. In addition, a simplified PI controller design based on indirect vector control is proposed in this paper. The current and the speed control loops on the dq-axis are designed to control the flux vector, torque, and speed. The simulation results ensure that the proposed PI parameter design is sufficient to provide the required PMSM speed. However, the problems with high oscillating torque and stator currents must be solved. For these issues, in order to obtain a decent transient response, the controllers in the current and the speed control loops should be modified. In the future work, an additional derivative term and a predictive mechanism must be developed.

ACKNOWLEDGEMENT

This work was supported by Faculty of Engineering, Prince of Songkla University (PSU).

References

[1] P. Pillay and R. Krishnan, "Control characteristics and speed controller design of a high performance PMSM," *1987 IEEE Power Electronics Specialists Conference*, pp. 598–606, 1987.

[2] G. D. Andreescu, C. E. Coman, A. Moldovan and I. Boldea, "Stable V/f control system with unity power factor for PMSM drives," *Proceeding of 13th IEEE International Conference on Optimization of Electrical and Electronic Equipment (OPTIM)*, pp. 432-438, 2012.

[3] A. Mishra, J. Makwana, P. Agarwal and S. Srivastava, "Mathematical Modeling and Fuzzy Based Speed Control of Permanent Magnet Synchronous Motor Drive," *Proceeding of 7th IEEE Conference on Industrial Electronics and Applications (ICIEA)*, pp. 2034-2038, 2012.

[4] B. Boazzo and G. Pellegrino, "Model Based Direct Flux Vector Control of Permanent Magnet Synchronous Motor Drives," *IEEE Transactions on Industry Applications*, Vol. 51, No. 4, pp. 3126-3136, 2015.

[5] P. Maji, G. K. Panda and P. K. Saha, "Field Oriented Control of Permanent Magnet Synchronous Motor Using PID Controller," *Advanced Research in Electrical. Electronics and Instrumentation Engineering*, Vol. 4, No. 2, pp. 632-639, 2015.

[6] G. Jayabaskaran, B. Adhavan and V. Jagannathan, "Torque Ripple Reduction in Permanent Magnet Synchronous Motor Driven by Field Oriented Control using Iterative Learning Control with Space Vector Pulse Width Modulation," *Proceeding of 2013 IEEE International Conference on Computer Communication and Informatics*, pp. 1-6, 2013.

[7] X. Wang, M. Reitz and E. E. Yaz, "Field Oriented Sliding Mode Control of Surface-Mounted Permanent Magnet AC Motors: Theory and Applications to Electrified Vehicles," *IEEE Transactions on Vehicular Technology*, Vol. 67, No. 11, pp. 10343-10356, 2018.

[8] X. Yuan, C. Zhang and S. Zhang, "Torque Ripple Suppression for Open-End Winding Permanent Magnet Synchronous Machine Drives with Predictive Current Control," *IEEE Transactions on Industrial Electronics*, Vol. 67, No. 3, pp. 1771-1781, 2019.

[9] X. Sun, M. Wu, G. Lei, Y. Guo and J. Zhu, "An Improved Model Predictive Current Control for PMSM Drives Based on Current Track Circle," *IEEE Transactions on Industrial Electronics*, Vol. 68, No. 5, pp. 3782-3793, 2020.

[10] H. Celik and T. Yigit, "Field-Oriented Control of the PMSM with 2-DOF PI Controller Tuned by Using PSO," *Proceeding of 2018 International Conference on Artificial Intelligence and Data Processing (IDAP)*, pp. 1-4, 2018.

[11] K. Tatemarsu, D. Hamada, K. Uchida, S. Wakao and T. Onuki, "New Approaches with Sensorless Drives," *IEEE Industry Applications Magazine*, Vol. 6, No. 4, pp. 44-50, 2000.

Nutthawut Kongchoo was born in Songkhla, Thailand, in 1997. He received the B.Eng. degree in Electrical Engineering from Prince of Songkla University (PSU), Songkhla, Thailand, in 2020. He is currently studying toward an M.Eng. degree in electrical engineering and works as a water supply officer in the Subdistrict Administrative Organization Tubchang, Songkhla, Thailand. His current research interests include control of motor drives, control of power electronics, simulation, and modeling.

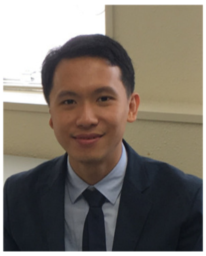

Phonsit Santiprapan was born in Ranong, Thailand, in 1988. He received the B.Eng., M.Eng., and Ph.D. degrees in Electrical Engineering from the Suranaree University of Technology (SUT), Nakhon Ratchasima, Thailand, in 2009, 2011, and 2016, respectively. Since 2017, he has been a lecturer in the department of electrical engineering at Prince of Songkla University (PSU), Songkhla, Thailand. In 2019, he was a visiting researcher at the University of Aizu, Fukushima, Japan. His current research interests include active power filters, unified power quality conditioning, power quality, artificial intelligence applications, simulation, modeling, and control of power electronics.

Nattha Jindapetch received the B.Eng. degree in Electrical Engineering from Prince of Songkla University, Thailand, in 1993, the M.Eng. in Information Technology, and the Ph.D. degree in Interdisciplinary Course on Advanced Science and Technology from the University of Tokyo, Japan in 2000 and 2004, respectively. She now is an Associate Professor at the Department of Electrical Engineering, Prince of Songkla University. Her research interests are FPGAs, embedded systems, and sensor networks.